Applied Nanoscience (2020) 10:2255–2268
https://doi.org/10.1007/s13204-020-01394-y

ORIGINAL ARTICLE

Enhanced antibacterial activity and photo-remediation of toxic dyes using Ag/SWCNT/PPy based nanocomposite with core–shell structure

Amanvir Singh[1] · Arkaja Goswami[2] · Sonia Nain[1]

Received: 19 February 2020 / Accepted: 4 April 2020 / Published online: 6 May 2020

Abstract

Water pollution has become a universal health problem due to frequently discharged toxic chemical effluents and contamination from pathogenic bacteria. Amidst all this, nanocomposites have gained wide interests owing to their promising application as photocatalysts and antibacterial agents. In the present study, hybrid Ag/SWCNT/PPy (Silver nanoparticles/Single-walled carbon nanotubes/Polypyrrole) based ternary nanocomposites were synthesized by applying facile and cost-effective one-pot synthesis approach. The morphological studies (SEM and TEM) revealed that the synthesized ternary nanocomposite possesses a core–shell type of structure where spherical Ag NPs anchored SWCNTs act as core and PPy formed a shell over it. The composites were also characterized by FTIR, XRD and UV. Ag/SWCNT/PPy was used as an efficient photocatalyst for degrading toxic organic dyes like RB (rose bengal) and MB (methylene blue). It showed high degradation rates of 91% and 89.3% against RB and MB dyes respectively within 100 min. of UV irradiation time. Owing to the synergistic effect of Ag NPs, SWCNTs and PPy, the synthesized ternary nanocomposite also inhibited the growth and multiplication of tested bacteria such as *S. aureus, B. cereus, E. coli and P. aeruginosa* completely within 24 h. Overall, Ag/SWCNT/PPy possesses a superior potential than Ag NPs and Ag/SWCNTs for their use in the development of photocatalysts and anti-bacterial agents, thereby paving a way for the treatment of wastewater and bio-remediation in near future.

Keywords Ternary nanocomposites · CNT-functionalization · Antibacterial agents · Photocatalysis · Toxic organic dyes

Introduction

Human population is rising exponentially and along with that its ever-rising demands for pure drinking water, disease-free environment and sustainable energy are challenging the researchers throughout the globe. The potential threat to world health today comes from disease-causing pathogens and toxic chemical effluents from industries that badly contaminate water, food and air. These pathogens are treated with antibiotics but with the passage of time, they undergo genetic modifications to develop resistance against a maximum number of antibiotics (Kümmerer 2009). On the other hand, the presence of harmful organic dyes in wastewater discharged by textile and photographic industries are among the major contributors to water pollution (Vajnhandl and Valh 2014). Therefore, the removal of these harmful dyes and pathogenic bacteria from our surroundings becomes the utmost priority for the survival of mankind. Till date, various metals as well as metal oxide-based nanocomposites have been employed effectively to tackle these issues (Franci et al. 2015; Zhang et al. 2013; Shaa et al. 2016; Sharma et al. 2018; Chahal et al. 2019; Tang et al. 2013), however, the complete eradication of this problem still remains a distant dream.

The nanocomposites are materials that provide emerging and promising research pathways for countering global issues related to sustainable energy, pure drinking water, flourishing environment etc. They are prepared by incorporation of nanosized particles into a standard matrix of two or more materials. Initially, each of the nanocomposite components has its unique properties but upon addition of nanoparticles, they show drastic improvements in mechanical properties (Kumar et al. 2015; Albdiry and Yousif 2014), antibacterial performance (Al et al. 2017; Yu et al.

✉ Sonia Nain
sonianain.chem@dcrustm.org

[1] Department of Chemistry, Analytical Lab, Deenbandhu Chhotu Ram University of Science and Technology, Murthal 131039, Haryana, India

[2] Department of Chemistry, Shyamlal College, University of Delhi, 110032 New Delhi, India

2015), catalytic behaviour (Pant et al. 2016; Magdalanea et al. 2016), thermal stability (Feng et al. 2011; Chen et al. 2012), energy storage (Xie et al. 2017; Yang et al. 2015; Suresh et al. 2019) etc. While designing a suitable nanocomposite, careful control of ingredient properties may lead to the synthesis of composites with enhanced photocatalytic, biocidal and supercapacitive properties. Recent studies have illustrated the use of small-sized AgNPs in nanocomposites as promising antimicrobial (Naz et al. 2019) as well as catalytic agents (He et al. 2018) for the degradation of harmful dyes. Due to the surface plasmonic resonance phenomenon (SPR), AgNPs directs the release of reactive oxygen species (ROS). These ROS form a huge number of free radicals which possess a powerful bactericidal action and degradation capability to degrade the dye molecules adsorbed on the surface of nanocomposite into lesser harmful by products. Furthermore, the release of Ag^+ ions from AgNPs enters the microbial body and causes irreversible damage to protein structure and prevents DNA replication (Hecel et al. 2019). The only drawback which AgNPs faces today is their tendency to agglomerate into large particles (Salmiati et al. 2017), which results in the deterioration of their unique properties. To overcome these problems, binary or ternary nanocomposites composed of AgNPs have been exhaustively studied.

Since their discovery by Iljima in 1991 (Yang et al. 2010), Carbon nanotubes have been successfully administered in many fields of science and technology like energy storage (Wu et al. 2017; Shi et al. 2014), catalysis (Gong et al. 2014; Wang et al. 2014), drug delivery (Digge et al. 2005; Dolatabadi et al. 2011), biosensing (Balasubramanian and Burghard 2006; Wang and Musameh 2005) etc. CNTs showed effectiveness in killing bacteria by disrupting their cell membrane. Due to their nano size and high specific surface area, CNTs can easily attack bacteria present in the medium and then forms Bacteria-CNT aggregate (Fig. 1). After the formation of aggregates with bacterial cell, CNTs damage and perturbate inside the cell wall of bacteria to release the bacterial cytoplasmic content and cause cell death (Ha et al. 2001). Kang et al. was first to prove that, SWCNTs show strong antibacterial activity against *E. coli* (Dizaj et al. 2015). They also reported later that SWCNTs are more effective than MWCNTs against pathogens$^+$. Accordingly, the synthesis of various CNT based nanocomposites demonstrates a promising approach for improved antibacterial activities (Kang et al. 2007).

Polypyrrole (PPy) is one of the most extensively studied conducting polymer due to its unique surface properties (Dubal et al. 2016; Huang et al. 2015; Wan and Li 2016; Bideau et al. 2016). Generally, conducting polymers (CPs) are a class of organic compounds that conduct electricity by virtue of their long π-conjugated chains. They are polycationic in terms of charge present on the surface and shows exceptional electrical and chemical properties. Apart from their applications in energy storage devices, they can also be used in bacterial resistance due to their highly

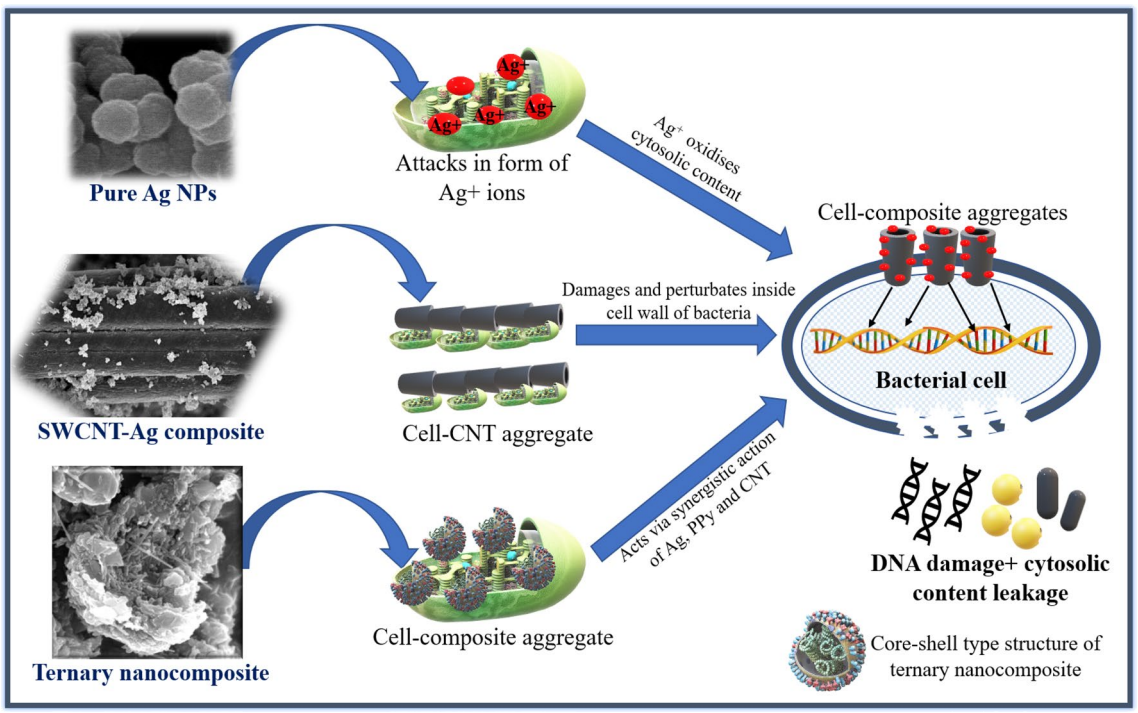

Fig. 1 Antibacterial activity mechanism of different nanomaterials incorporated in Ag/SWCNT/PPy

charged surface (Maruthapandi et al. 2019; Salahuddin et al. 2017; Cabuk et al. 2014). This charged surface develops electrostatic interaction with oppositely charged bacterial extracellular organelles and finally promotes bacterial cell death. Considering their good microcidal effects, one could enhance the bacterial resistance of CPs by improving their surface potential. Polypyrrole is one such conducting polymer that can withstand all these expectations. It is also easy to synthesize and exhibits improved charge storage and mechanical strength when fabricated with carbon nanomaterials (Sasso et al. 2010; Kang et al. 2019).

There are many research studies devoted to the synthesis of different binary or ternary nanocomposites based on AgNPs (Masumeh et al. 2016; Jia et al. 2014), SWCNTs (Abdi et al. 2017; Rajendran et al. 2014) and PPy (Amirul et al. 2018; Duan et al. 2016). But to the best of our knowledge, there is minimal work available in literature which is solely focused on synthesizing a ternary nanocomposite based on these three nanomaterials for multifunctional activities. Consolidation of different nanomaterials together to form ternary nanocomposite of Ag/SWCNT/PPy would synergies the antibacterial and photocatalytic effects, and minimize the ill effects of these nanomaterials. In the present study, Ag/SWCNT/PPy based ternary nanocomposite was synthesized and its potential use in the fields of wastewater remediation and bacterial removal were explored.

Materials and methods

Chemicals and reagents

For synthesizing ternary nanocomposite, SWCNTs (OD 1–2 nm and average length 3–8 μm) were obtained from Nanoshel (USA). Analytical grade silver nitrate ($AgNO_3$, 99%), Hydrazine hydrate (N_2H_4, 80%), sodium dodecyl sulfate (SDS, 99%), absolute ethanol (C_2H_5OH), Hydrochloric acid (HCl) and pyrrole monomer (C_4H_5N, 98%) were purchased from Merck and were used as received.

Microorganisms

Bacterial strains were procured from MTCC (Microbial Type Culture Collection) Chandigarh, India. Two Gram-positive bacteria; *Staphylococcus aureus* (MTCC 11,949) and *Bacillus cereus* (MTCC 1272) and two Gram-negative bacteria; *Escherichia coli* (MTCC 9721), *Pseudomonas aeruginosa* (MTCC 3542) were used in the present study. Tetracycline was used as a positive control whereas ethanol which was preferred for dispersing the nanocomposites served as a negative control.

Synthesis of silver nanoparticles

As shown in Fig. 2, Ag NPs were synthesized via chemical reduction method using silver nitrate as a metal precursor. Initially, a solution of $AgNO_3$ (2.8 g, 16.48 mmol) was prepared in (100 mL) ethanol. Then, 1.5 g of sodium dodecyl sulfate were added to the solution to prevent agglomerations. After that, it was ultrasonicated for 60 min and simultaneously stirred at the rate of 1000 rpm for 12 h. Dropwise addition of hydrazine hydrate (2 mL) was carried out. During the additional time, change in color from black to grey indicated the formation of silver nanoparticles inside the beaker. The resulting precipitates were centrifuged and washed several times with distilled water to get rid of residual surfactant completely from the solution. Finally, silver nanoparticles were obtained by drying the above mixture overnight at 50 ºC in oven.

The probable stepwise chemical reactions occurring during the formation of silver nanoparticles are as follow:

$$AgNO_3 \rightleftharpoons Ag^+ + NO_3^-, \tag{1}$$

$$Ag^+ + \text{anionic surfactant} \rightarrow n\left[\text{surfactant}^-\left(Ag^+\right)\right], \tag{2}$$

$$Ag^+ + N_2H_4(\text{Hydrazine hydrate}) \rightarrow Ag\left(N_2H_4\right)^+, \tag{3}$$

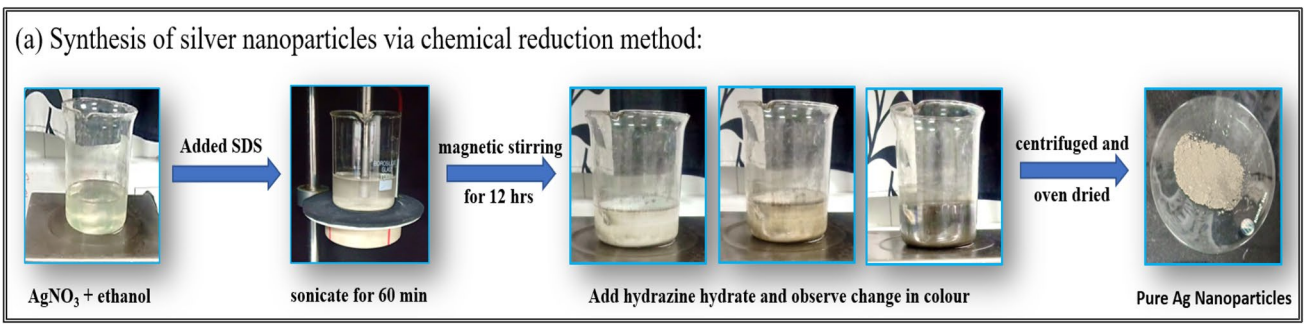

Fig. 2 Synthesis of Ag NPs via facile chemical reduction method

$$Ag\left(N_2H_4\right)^+ + N_2H_4 \rightarrow Ag^0 + N_2(gas) + NH_3 + NH_4^+, \quad (4)$$

Fabrication of Ag/SWCNT/PPy nanocomposite

As demonstrated in Fig. 3, 0.36 g of activated SWCNTs were dispersed in 100 mL ethanol and sonicated by a probe sonicator for 60 min. Then 0.15 g of the above prepared Ag NPs were added to this solution. The resulting mixture was again sonicated for another 80 min. with simultaneous magnetic stirring for 08 h. The sonicated solution was then centrifuged and the precipitates were oven-dried at temperatures not exceeding 100 ºC to obtain Ag/SWCNT nanocomposite.

In a buerette, 0.3 g (4.47 mmol) of pyrrole was dissolved in 50 mL of 1 M HCl. To prevent side reactions of pyrrole, the temperature of the solution was maintained below 4 ºC while adding pyrrole monomer. Now the appropriate amount of above-prepared binary composite (60% *w*/*w* of pyrrole) was dispersed in ethanol in a separate beaker. Then pyrrole solution was added dropwise to the binary composite through buerette. The resultant mixture was magnetically stirred for 60 min. and then kept untouched for 24 h. for complete oxidation of pyrrole. Thenceforth, the precipitates were collected and washed properly with distilled water 3–4 times, later oven dried at 50 ºC to obtain Ag/SWCNT/PPy based ternary nanocomposite.

Antibacterial activity assay

The antibacterial activity of the synthesized nanocomposite was evaluated against selected Gram-positive and Gram-negative bacterial strains using agar well diffusion method (Kaushik et al. 2019). The activity was assessed in terms of size of diameter in the zone of inhibition and minimum inhibitory concentration (MIC) which was calculated using the broth dilution method.

Minimum inhibitory concentration measurements

MIC of the prepared nanocomposites against selected gram-positive and gram-negative bacterial strains was calculated using a previously reported Broth dilution method (Fig. 4). Briefly, 2 mL aliquots of sterile Mueller Hinton broth were taken in sterile tubes. Then, 2 mL of nanocomposite suspension (25 mg/mL) was added in the first tube, followed by diluting 2X times in each tube. Subsequently, 100 µL of bacterial culture was inoculated in each tube and incubated at 37 ºC for 24 h. The lowest nanocomposite concentration that gave no visible bacterial growth after 24 h. was recorded as MIC value for that particular composite.

Photo-catalytic activities assays

RB and MB dyes were selected to compare the photocatalytic degradation potential of synthesized Ag/SWCNT/PPy based ternary nanocomposite with its Ag/SWCNT based binary precursor. The degradation experiments were performed under two UV irradiated dark chambers, each fitted with single UV light bulb (300 W/bulb with $\lambda = 365$ nm). Each composite was analyzed against both the dyes on one particular day. The average temperature during the experiment was found to be around 24 ºC. Every day, before starting the experiment, 0.07 g of the synthesized photocatalyst was added separately to two beakers carrying

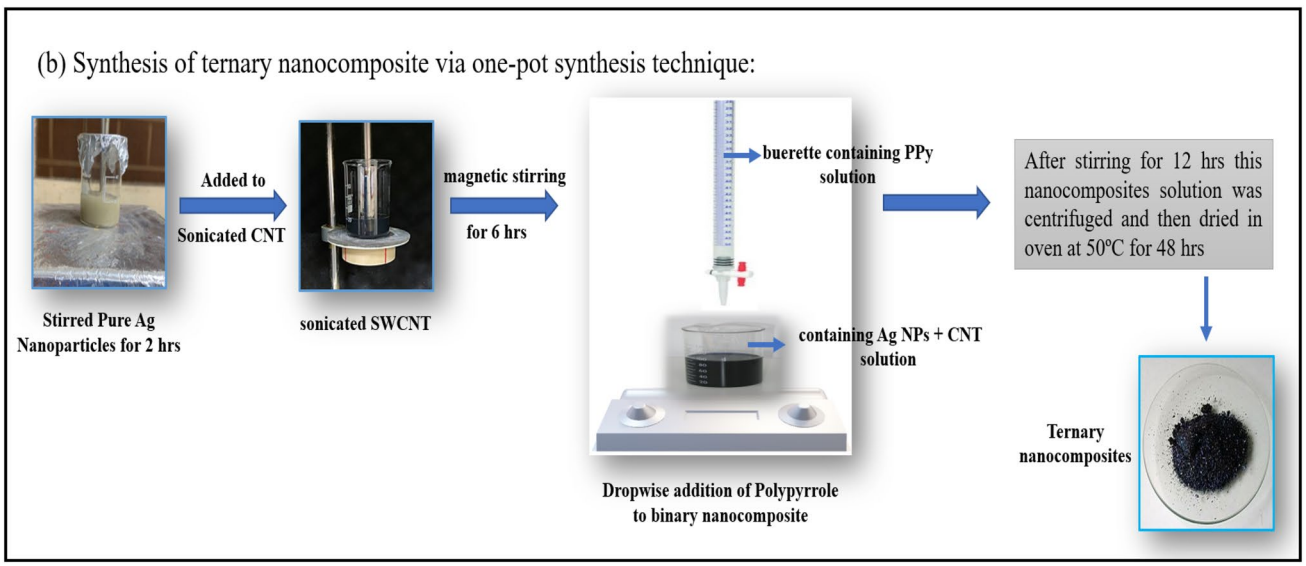

Fig. 3 Schematic diagram of steps involved in the synthesis of Ag/SWCNT/PPy based ternary nanocomposites

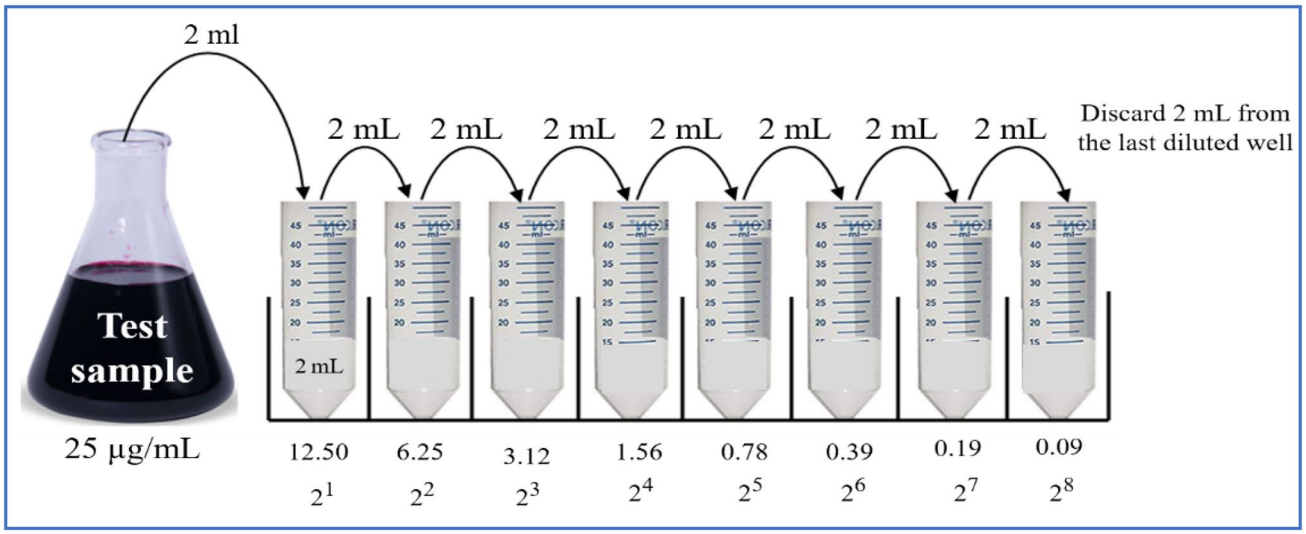

Fig. 4 Schematic diagram of Broth dilution method

70 mL solution of 10 ppm RB and MB dyes respectively. The mixtures were first stirred constantly at 1200 rpm for 60 min in complete darkness to ensure in-situ adsorption–desorption equilibrium between dye molecule and catalyst surface. After equilibrium attainment, the beakers were placed over continuous magnetic stirring for 100 min inside different UV irradiated chambers. A small amount of aliquot was collected at a gap of every 20 min from the beakers. These extracted aliquots were centrifuged at 4000 rpm for 5 min to obtain clean supernatant. The absorption spectrum of the supernatant was then analyzed periodically using UV–vis spectrophotometer for leftover dye concentration.

The degradation efficiency and half-life time (Chahal et al. 2020) of above-mentioned dyes was calculated using the following formulae:

$$\text{Degradation efficiency } (\%) = \frac{C_0 - C_t}{C_0}, \tag{5}$$

$$\frac{\ln C}{C_0} = kt, \tag{6}$$

$$t_{1/2} = \ln 2/k, \tag{7}$$

where C_0 represents the initial concentration of dyes after equilibrium, C_t represents the concentration after periodic degradation of dyes and $t_{1/2}$ represents half life time i.e. time taken to degrade the dye up to half of its initial concentration.

Results and discussion

FTIR spectra

This qualitative technique was performed on NICOLET 5700-Fourier Transform Infrared (FTIR) spectrometer using KBr method. As depicted in Fig. 5, both the spectra represent almost similar broad absorption band in the range 3600–3200 cm^{-1} due to the presence of O–H, C–H/N–H groups within the composites. Appearance of the striking peak at 2920 cm^{-1} (due to C–H stretchings), 1020 cm^{-1} (due to C–O stretchings) and noticeable bumps

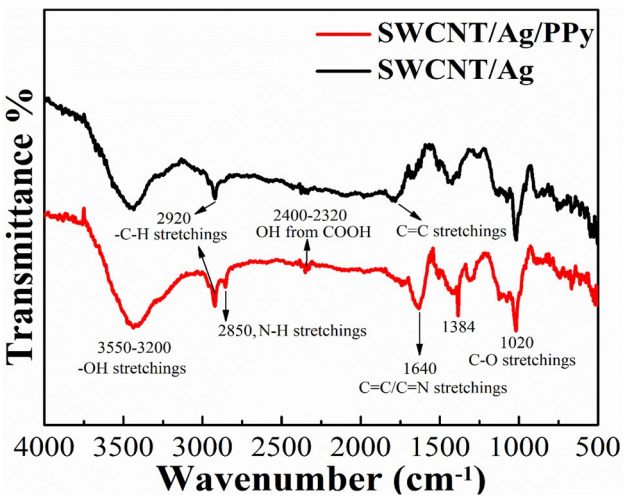

Fig. 5 IR data of Ag/SWCNT and Ag/SWCNT/PPy based nanocomposites

in the range 2400–2320 cm^{-1} persuades that both composites contain acid-treated SWCNTs as one of their components. Interestingly, the appearance of the low shoulder near 1700–1620 cm^{-1} (due to C=C bond stretchings) in the spectra of Ag/SWCNT got intensified on the addition of PPy which further introduced strong intra-chain C=N/C=C stretching vibrations within Ag/SWCNT/PPy nanocomposite. Moreover, the appearance of prominent peaks at 2850 cm^{-1} (due to N–H stretchings), 1384 cm^{-1} (correspond to N–H stretching vibrations of aromatic amines) and 1640 cm^{-1} strongly advocates for the presence of covalently bonded nitrogen in highly interconnected core of carbon chains.

X-ray diffraction analysis

The X-ray diffraction (XRD) was performed by Rigaku X-Ray Diffractometer using CuKα X-ray source (λ = 1.5406 Å). The XRD patterns of pure Ag NPs, Ag/SWCNT and Ag/SWCNT/PPy are shown in Fig. 6. The high intensity and sharp nature of peaks implied that all the synthesized composites were highly crystalline in nature. Peaks located at $2\theta = 38.2°$, 44.4°, 64.5° and 77.5° corresponds to the face-centered cubic (FCC) structure of Ag NPs. All these peaks are associated with (111) (200) (220) and (311) crystallographic planes of Ag NPs respectively. This observed data is in complete agreement with JCPDS [card no. 03-0931]. A broad peak observed at 26.2° in Ag/SWCNT composite corresponds to (002) plane of graphitic carbon. Apart from the peaks of Ag NPs and CNTs (as discussed above), a slight hump in the curves of Ag/SWCNT/PPy composite from baseline up to 20° was observed due to amorphous structure of polypyrrole pointing towards the homogeneous dispersion of PPy on CNT surface. No obvious diffraction peaks for CNTs are observed in the ternary nanocomposite because the regular carbon stack of these nanomaterials is damaged due to interaction of PPy with CNTs. It is also evident from Fig. 6, that upon introduction of CNT or PPy, all the peaks for Ag NPs showed a minor shift in their diffraction angles, which finally induce variation in interplanar spacing (*d*). Crystallite size (D) was calculated using Scherrer's equation: $D = k\lambda/\beta\cos\theta$ for both composites (tabulated in Table 1). The average crystallite size was found 37 nm, 35 nm and 32 nm for Ag NPs, Ag/SWCNT, Ag/SWCNT/PPy respectively when calculated using Scherrer's equation on Ag (111) peak. This variation in average crystallite size can be attributed to the stepwise addition of different carbon nanomaterials during the synthesis of binary and ternary composites.

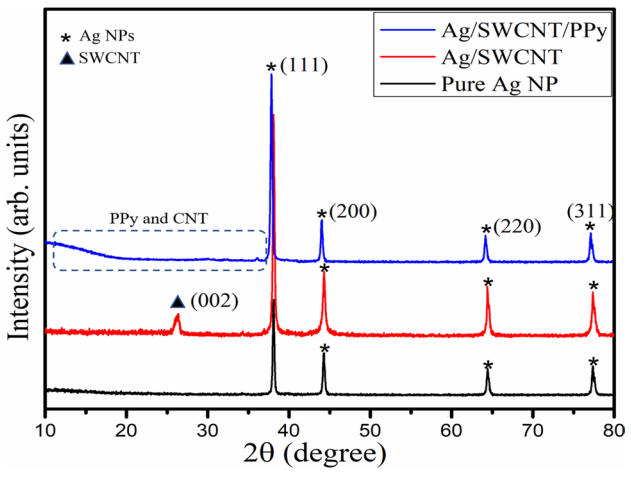

Fig. 6 XRD patterns of pure Ag NPs, Ag/SWCNT and Ag/SWCNT/PPy nanocomposites

Microstructural analysis

To further justify the synthesis and anchoring of Ag NPs on SWCNTs within PPy shell, scanning electron microscopy (SEM) and Transmission electron microscopy (TEM) were performed using Carl Zeiss NTS Ltd. (PHI 5000 Versa Probe II FEI Inc.) and Thermoscientific-Talos TEM respectively. Figure 7, depicts the fine attachment of a large number of Ag NPs on the surface of SWCNTs. These anchored nanoparticles are smaller in size and possess quasi-spherical shapes. Also, TEM images elucidate that Ag NPs showed slight morphological changes in Ag/SWCNT composites (Fig. 8), the silver nanoparticles turned nearly elliptical in shape due to the presence of infinite nucleation sites within amorphous layers of SWCNTs. Interestingly, both the microscopic studies collectively revealed the formation of a core–shell type of structures upon the incorporation of PPy. This core–shell kind of interaction between SWCNTs and PPy could be attributed to the formation of charge-transfer complex between them, where SWCNTs acts as electron-acceptor core and PPy plays the role of electron-donor shell.

Furthermore, the particle size and morphology of pure Ag NPs and Ag/SWCNT based binary nanocomposite were analyzed by TEM. The average particle size evaluated from these images lies near 37 nm for pure Ag NPs and between 34 and 36 nm for Ag/SWCNTs. Also, the particle size distribution histograms (inset of Fig. 8a, b) show that the size

Table 1 Various parameters calculated from XRD data of synthesized binary nanocomposites

For (111) plane of Ag Nanoparticles	2 θ (observed)	*d* (in nm)	*D* (in nm)
Pure Ag NPs	38.1007	2.361	37.042
SWCNT-Ag	38.1122	2.358	35.612
SWCNT-Ag-PPy	38.8438	2.376	32.478

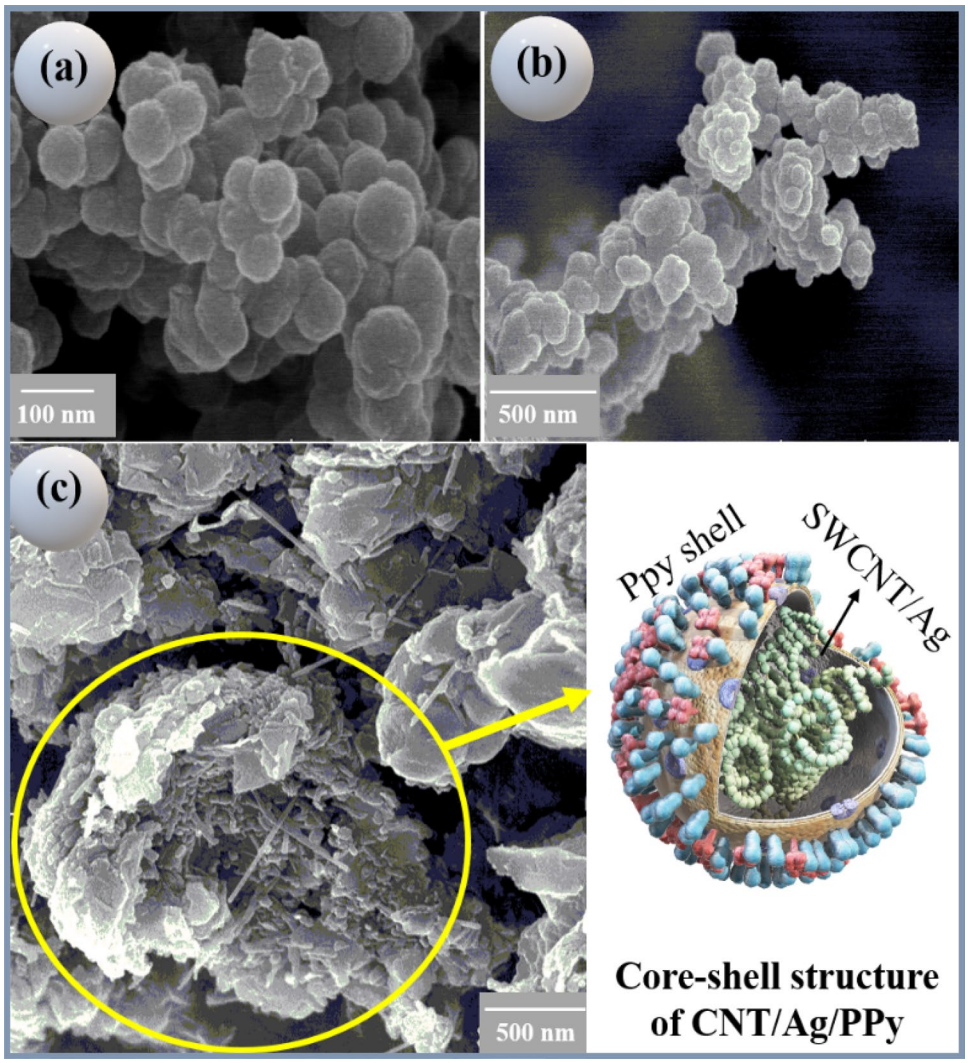

Fig. 7 FESEM images of **a** pure Ag NPs, **b** Growth of Ag NPs in their respective planes, **c** core–shell structure of Ag/SWCNT/PPy based ternary nanocomposite

distribution of Ag NPs lies in a quite narrow range. This aggregation of particles within such a short size range indicates that the synthesized particles are nanocrystalline in nature. All these results are in corroboration with the values obtained from XRD analysis. It can be clearly observed from Table 1, that the crystal growth remained almost consistent as we move from pure Ag NPs to Ag/SWCNT/PPy composites, however, the morphology of anchored Ag NPs manifested a change from spherical to nearly elliptical. This predomination of small-sized nanoparticles within both the composites may enhance their photocatalytic as well as antibacterial properties.

Antibacterial investigation of Ag/SWCNT/PPy

The antibacterial activity of synthesized nanocomposite was evaluated against selected bacterial strains through agar well diffusion assay (Fig. 10). It was observed that Ag/SWCNT/PPy nanocomposite was highly effective against *B. cereus* with 19 mm diameter of zone of inhibition (ZOI) followed by *E. coli* with 18 mm ZOI (Fig. 9). However, least activity was depicted against methicillin-resistant *S. aureus* for obvious reasons. This enhancement in antibacterial potential of Ag/SWCNT/PPy composite could be attributed to the synergistic effect of all the three components. As depicted in Fig. 9, pure Ag NPs alone possess an appreciable amount of activity against both gram-positive and gram-negative bacterial strains. As Ag NPs approach the bacterial cell, they generate reactive oxygen species via SPR phenomenon (Liang et al. 2018). These ROS are generally free radicals with powerful antibacterial action. Further, these free radicals along with Ag^+ ions from Ag NPs bind with thiol groups present in enzymes and proteins to create huge disturbance in cellular functionalities. Such disturbances cause irreparable damages to DNA replication ability of bacteria and finally leads to bacterial cell death (Ahn et al. 2014). Moreover, the small size of these Ag NPs helps them to easily cross the intercellular membrane of pathogenic bacteria. On the other

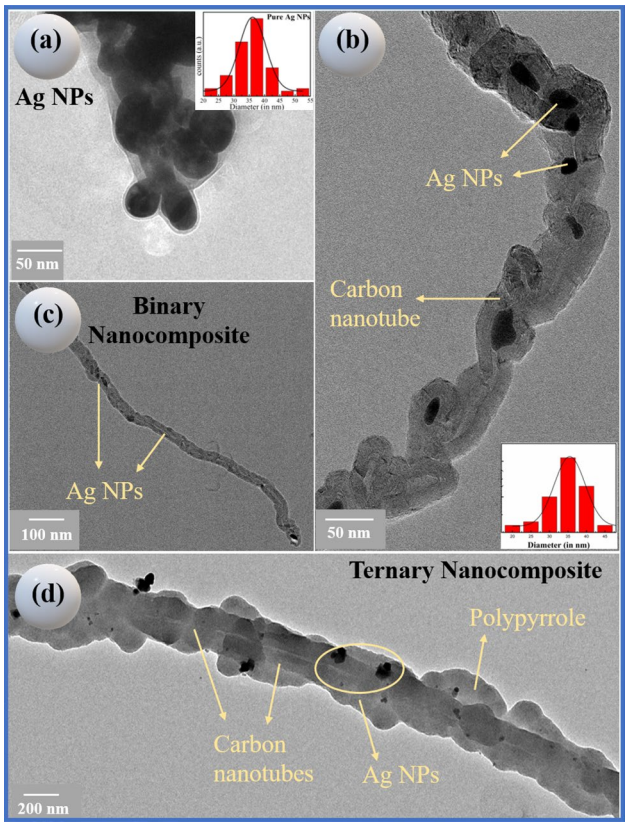

Fig. 8 TEM images of **a** pure Ag NPs, **b**, **c** Ag/SWCNT based binary nanocomposite, **d** covering of Ag/SWCNT core by polypyrrole shell

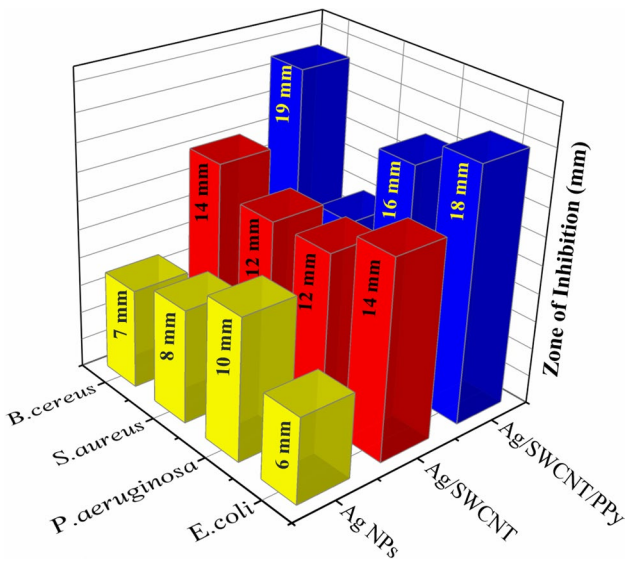

Fig. 9 Diameter of zone of inhibition of Ag NPs, Ag/SWCNT, Ag/SWCNT/PPy nanocomposite against different gram-positive and gram-negative bacterial strains

hand, the presence of SWCNT and PPy synergistically provide a huge surface for facile attack followed by elimination of bacteria present inside the medium. Due to their hollow structure and sharp edges, SWCNT traps the bacteria inside and form Bacteria-CNT aggregates. After the formation of these aggregates, SWCNTs produce a significant amount of stress on trapped bacterial body which leads to rupturing of cell membranes and causing the bacterial death due to leakage of cytoplasmic content. In case of Ag/SWCNT composite, the Bacteria-CNT aggregate formation also provides ample time for Ag NPs attached on SWCNTs to attack and disintegrate the bacterial membranes. As represented in Fig. 9, upon the incorporation of PPy, a significant increase in antibacterial activity of nanocomposite was observed. The ZOI diameter values increased by 4 mm in *P. aeruginosa* and *E. coli* on treatment with Ag/SWCNT/PPy (Fig. 10). This increased antibacterial activity of ternary nanocomposite could be attributed to good dispersion of Ag NPs on the CNTs surface that supported the synergistic action of SWCNTs, Ag NPs and polycationic surface of the conducting polymer. The charged surface of polypyrrole develops electrostatic interactions with oppositely charged bacterial extracellular organelles and finally promotes cell death by providing enough time for both SWCNTs and Ag NPs to attack these electrostatically attracted cell organelles.

To further validate the obtained results, MIC was calculated using 2X Broth dilution method. From the results of this experiment, it was observed that synthesized Ag/SWCNT/PPy nanocomposite showed least MIC value of 0.048 mg/mL against both *E. coli* and *B. cereus.* However, the binary nanocomposite without PPy showed least MIC values of 0.195 mg/mL against these two bacterial strains. As shown below (Table 2), pure Ag NPs were found to be highly effective against *P. aeruginosa* with MIC value of 0.390 mg/mL in comparison to other selected bacterial strains. Hence, the observed results of MIC values are in well corroboration with those obtained from agar well diffusion assay (ZOI) and finally confirms that the synthesized ternary nanocomposite showed improved antibacterial activity by attacking the bacterial intracellular and extracellular membranes, leading to disturbances in their cellular functionalities and DNA replications.

Photocatalytic degradation of toxic dyes

Mechanism involved

Before UV irradiation, the dye molecules were allowed to adsorb randomly on the surface of the catalyst to establish an adsorption–desorption equilibrium between the dye molecules and catalyst surface. Now upon irradiation, all the spherical Ag NPs already present in the core of Ag/SWCNT/PPy based catalyst absorb UV light. By absorbing the photons with energy

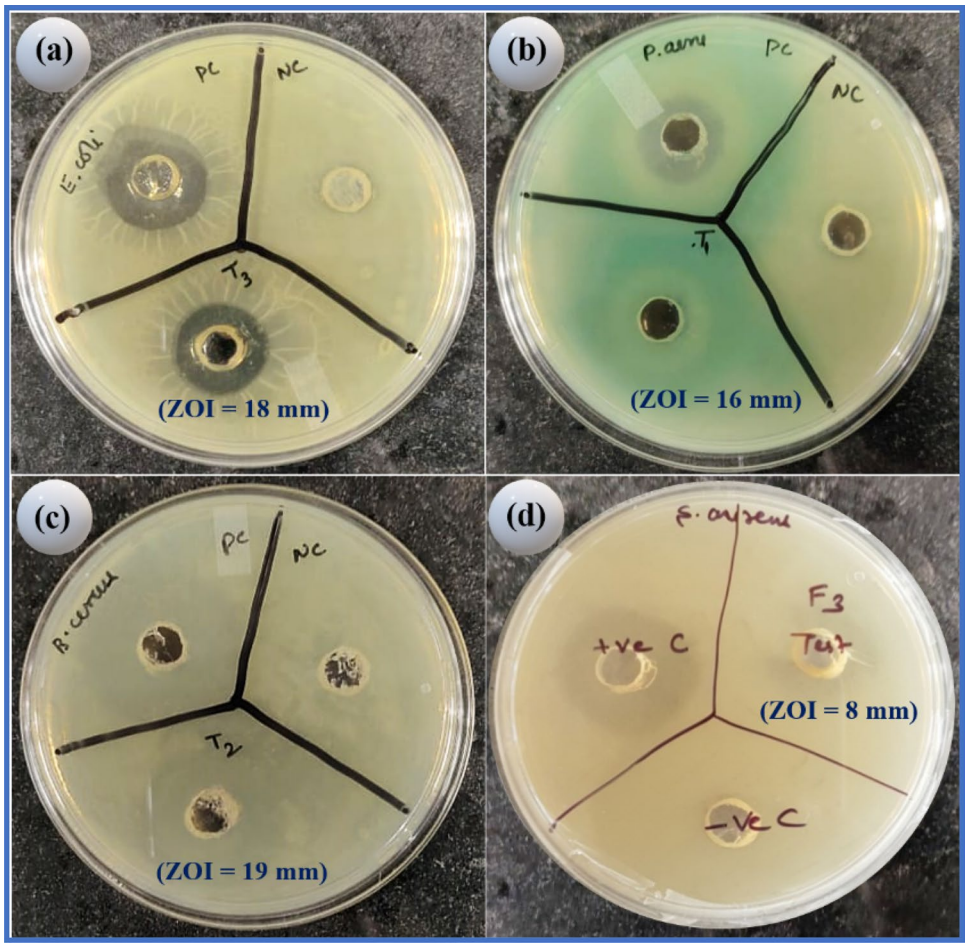

Fig. 10 Antibacterial activity of Ag/SWCNT/PPy based ternary nanocomposite showing zone of inhibition against. **a** *Escherichia coli*, **b** *Pseudomonas aeruginosa,* **c** *Bacillus cereus* and **d** *Staphylococcus aureus*

Table 2 MIC (Minimum Inhibitory Concentration) values of synthesized nanocomposites against different bacterial strains

S. no	Bacterial strains	CNT/Ag/Ppy Nanocomposites	CNT/Ag Nanocomposites	AgNPs
1	*E. coli* (MTCC 9721)	0.048	0.195	0.781
2	*P. aeruginosa* (MTCC 3542)	0.097	0.390	0.390
3	*S. aureus* (MTCC 11,949)	0.390	0.390	1.562
4	*B. cereus* (MTCC 1272)	0.048	0.195	0.781

higher than the value of band gap, an electron–hole pair is generated within the catalyst, thus rendering the photovoltaic effect (Wang et al. 2018a). The absorbed photons directly lead to excitation of valence electrons present in 4 *d* band to 5 *sp* band (blue lines in Fig. 11) and other higher energy states through SPR phenomenon (Chen et al. 2010). These photoexcited electrons are then trapped and transported within highly interconnected channels of carbon nanotubes and polypyrrole, leaving behind holes (h^+) at their respective sites. The trapped electrons can further facilitate the holes created after photo-excitations to be swept away in semiconductor channels (Wang et al. 2018b), where they show greater affinity for accepting electrons from dissolved O_2 and H_2O molecules. As shown in Fig. 12, these interactions further result into the generation of highly unstable Reactive Oxygen Species (ROS) that attack and break down the dye molecules adsorbed on huge surface of ternary nanocomposite into carbon dioxide and water (Eq. 14).

This proposed mechanism for dye degradation can be understood by the following equations:

1. Initial adsorption–desorption equilibrium set up

$$\text{Dye molecules} + \text{ternary composite} \leftrightarrow \text{Dye molecules/ternary comp.} \quad (8)$$

(where ternary composite represents Ag/SWCNT/PPy based photocatalyst).

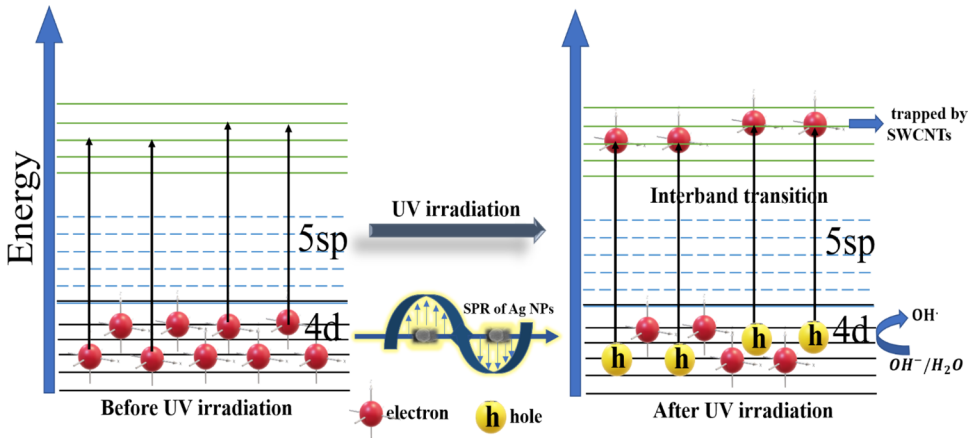

Fig. 11 Schematic energy diagram of Ag NPs present inside the core of photocatalyst

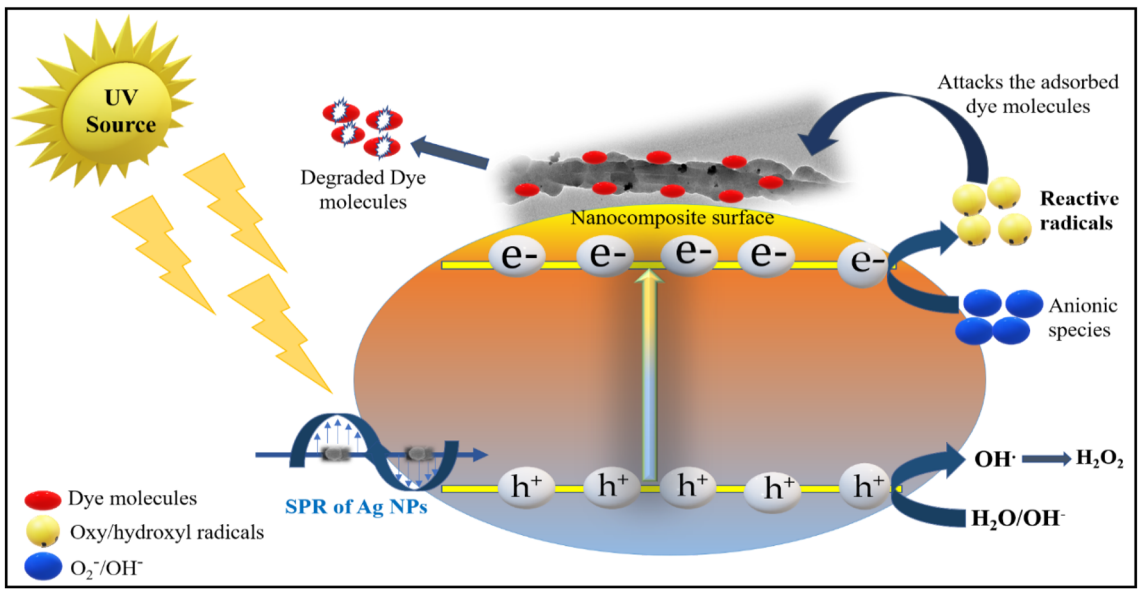

Fig. 12 Proposed photocatalytic mechanism for degradation of toxic dyes

2. Absorption of photons by photocatalyst

$$\mathrm{Ag-SWCNT-PPy/Dye\ molecules} + h\nu \rightarrow (\mathrm{Ag-SWCNT-PPy/Dye})^{+} + e^{-}. \quad (9)$$

3. Generation of ROS (Reactive Oxygen Species)

$$O_2 + e^- \rightarrow O_2^{\cdot -}\ \text{(superoxide radical)}, \quad (10)$$

$$O_2^{\cdot -} + H^+ \rightarrow HOO^{\cdot}\ \text{(perhydroxyl radical)}, \quad (11)$$

$$OH^- + \text{holes}\left(h^+\right) \rightarrow OH^{\cdot}\ \text{(hydroxyl radical)}, \quad (12)$$

$$OH^{\cdot} + OH^{\cdot} \rightarrow H_2O_2\ \text{(peroxide)}. \quad (13)$$

4. Degradation step

$$\mathrm{ROS}\left(O_2^{\cdot -}, OH^{\cdot}, H_2O_2\right) + \text{adsorbed dye molecules} \rightarrow H_2O + CO_2 + \text{degraded dye} \quad (14)$$

Figure 13a, b represents the UV absorption spectrum for degradation of RB dye using Ag/SWCNT and Ag/SWCNT/PPy based nanocomposites as photocatalysts. The absorption peak for RB appeared at 550 nm and then shifted to the lower side with extension in UV exposure time. This gradual decrease in intensity of the absorption peak upon UV irradiation proves that the dye is being degraded by the

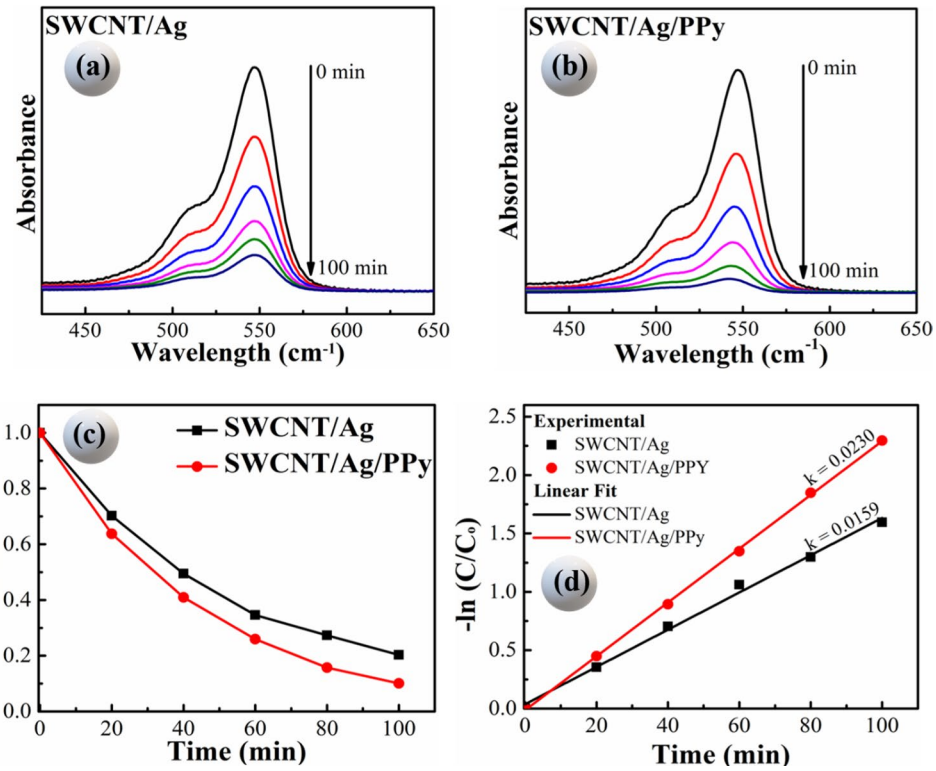

Fig. 13 Absorbance of RB dye with **a** Ag/SWCNT, **b** Ag/SWCNT/PPy at different time intervals, **c** C/Co versus degradation time for different nanocomposites under study for RB dye, **d** experimental and linearly fitted plots of $-\ln(C/C_0)$ with UV illumination time

Table 3 Parameters calculated from photodegradation of RB and MB dyes using both the synthesized binary and ternary nanocomposites

Samples	Rose Bengal		Methylene blue	
	K (min^{-1})	R^2	K (min^{-1})	R^2
Ag/SWCNT	0.0159	0.989	0.0218	0.983
Ag/SWCNT/PPy	0.0230	0.995	0.0134	0.992

catalyst with the passage of time. As demonstrated, the percentage degradation for Ag/SWCNT was 79.8%, whereas Ag/SWCNT/PPy composite degraded the RB dye up to 91%. A plot of $-\ln(C/C_0)$ with UV illumination time was plotted to find out the rate constant k, these values of k were further utilized for the estimation of half-life time. The values of the linear correlation coefficient (R^2) were also found very close to unity. All this data is presented in Table 3 and is sufficient to prove that the degradation process followed pseudo first-order kinetics equation.

To further support the obtained results, careful experiments were performed with MB dye (Fig. 14). The characteristic absorption peak at 650 nm was considered for examining the degradation potential of the synthesized catalysts. These peaks also accompanied a descending pattern with UV exposure time. After observing the final results, it can be concluded that again Ag/SWCNT/PPy dominated over binary composite and degraded MB dye by 89.3% within 100 min of UV irradiation. This comparatively better degradation capability in case of ternary nanocomposite with both the dyes can be attributed to several structure and interaction related factors. In comparison to its binary counterpart, Ag/SWCNT/PPy has a huge surface that provides ample opportunity for dye molecules to adsorb over it. More the number of adsorbed molecules then greater are the chances of their reaction with free radical species. The symmetric as well as strong superficial interaction of Ag NPs with CNTs and PPy escalates the smooth generation of ROS via SPR phenomenon. Besides all these, Ag/SWCNT/PPy also showed highly reinforced charge transfer through its interconnected carbon channels that led to increment in electron–hole recombination time. As shown in Table 3, the rate constant k and R^2 for RB and MB dyes were also evaluated after linear fittings of the plot between $-\ln c/c_0$ and degradation time and it yet again established that all the dye degradation processes performed here followed pseudo first-order kinetics as R^2 values lie between 0.95 and 1.

Effect of temperature

Based on the hypothesis; increase in temperature leads to an increase in kinetic energy of the molecules which further enhances their collisions with the catalyst surface. If the catalyst surface is very active so numerous free radicals will be present in the moiety surrounding the photocatalyst, so fast degradation of the dye molecules will take place (Barakat et al. 2013). However, contrary to it, increase in

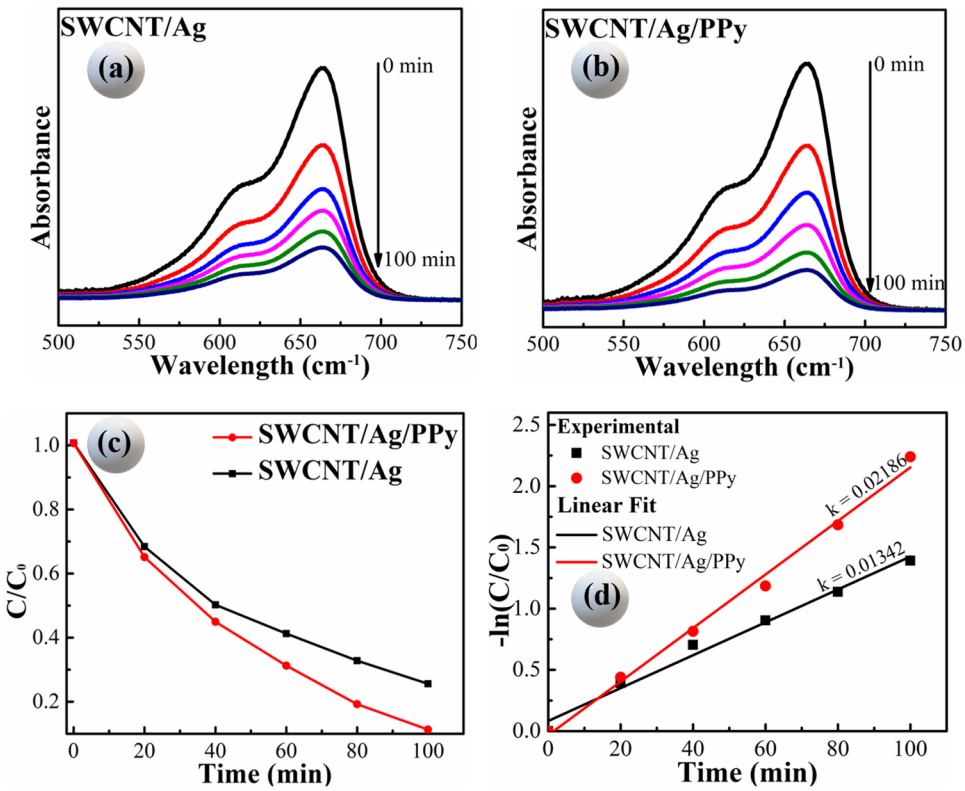

Fig. 14 Absorbance of MB dye with **a** SWCNT/Ag, **b** SWCNT/Ag/PPy at different time intervals, **c** C/Co versus degradation time for different nanocomposites under study for RB dye, **d** experimental and linearly fitted plots of $-\ln(C/C_0)$ with UV illumination time

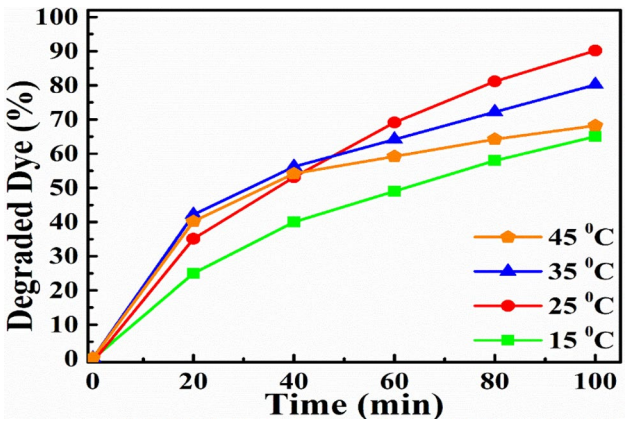

Fig. 15 Photodegradation of rose bengal dye using Ag/CNT/PPy based photocatalyst at different temperature conditions

temperature also enhances electron–hole recombination and desorption process of the adsorbed dye molecules, resulting in poor photodegradation ability of the catalyst (Saravanan et al. 2017).

Figure 15, displays the photodegradation of rose bengal dye using Ag/SWCNT/PPy based photocatalyst at different temperatures. The photocatalyst has a distinct performance at temperatures above 25 °C. The catalyst degraded almost 56% of the dye within first 40 min. of its inception at higher temperatures, but as the reaction proceeded, a gradual decrease in the degradation tendency was observed and it ended up with 72% and 64% degradation of the dye at 35 °C and 45 °C, respectively. Overall, maximum degradation rates were obtained at 25 °C, as the catalyst degraded 91% of rose bengal dye within 100 min. of UV irradiation time. These obtained results can be explained by aforementioned hypothesis that, the photodegradation of dyes cannot be mathematically correlated with the reaction temperatures as it is mainly based on electrons transfer process and amount of dye adsorption on the surface of photocatalyst. Therefore, increase in temperature influences the rate of degradation only up to a limited temperature range (25–30 °C in the case of Ag/CNT/PPy) by modifying the activation energy and collision frequency. But after this optimum range, further increase collectively affects the electron–hole recombination lifetime and desorption of dye molecules from the active surface of the catalyst that finally leads to lower degradation rates.

Conclusion

Hybrid Ag/SWCNT/PPy based multifunctional ternary nanocomposite was synthesized via facile one-pot synthesis approach. The morphological studies revealed good affinity among the synthesized nanocomposite, where Ag/SWCNT appeared as core, shelled by PPy. Compared to

pure Ag NPs and SWCNT/Ag, the synthesized ternary nanocomposite with an optimal ratio of SWCNT to Ag NPs is much more effective and shows synergistically enhanced, strong antibacterial activities at rather low dose (0.048 mg/mL). The diameter of ZOI and MIC values further confirmed that Ag/SWCNT/PPy exhibit more toxicity against E. coli than that to S. aureus. Interestingly, the ternary nanocomposite also decolorized harmful organic dyes like RB and MB by 91% and 89.3%, respectively within 100 min. of UV irradiation time. These findings suggest that the synthesis of Ag/SWCNT/PPy based ternary nanocomposite can not only photo-catalytically degrade toxic or harmful organic dyes but also proved efficient against both Gram-positive and Gram-negative bacteria. Hence, this new pathway for exploiting CNT-based ternary nanocomposites could ultimately advance logical fabrication techniques of carbon nanotubes not only for artificial photosynthesis or biocidal effects but also for numerous unknown prospective related to these "future materials".

Acknowledgements One of the authors, Amanvir Singh is thankful to CSIR (New Delhi), for providing financial support under SRF scheme. The authors would also like to acknowledge SAIF AIIMS (New Delhi) and Central Instrumentation Laboratory (CIL), Deenbandhu Chhoturam University of Science and Technology, Murthal for providing instrumentation facilities.

References

Aani SA, Virginia A, Chris G, Wright CJ, Hilala N (2017) Fabrication of antibacterial mixed matrix nanocomposite membranes using hybrid nanostructure of silver coated multi-walled carbon nanotubes. Chem Eng J 326:721–736

Abdah MA, Razali NS, Lim PT, Kulandaivalu S, Sulaiman Y (2018) One-step potentiostatic electrodeposition of polypyrrole/graphene oxide/multi-walled carbon nanotubes ternary nanocomposite for supercapacitor. Mater Chem Phys 219:120–128

Abdi J, Vossoughi M, Mahmoodi NM, Alemzadeh I (2017) Synthesis of metal-organic framework hybrid nanocomposites based on GO and CNT with high adsorption capacity for dye removal. Chem Eng J 326:1145–1158

Ahn JM, Eom HJ, Yang X, Meyer JN, Choi J (2014) Comparative toxicity of silver nanoparticles on oxidative stress and DNA damage in the nematode, *Caenorhabditis elegans*. Chemosphere 108:343–352

Albdiry MT, Yousif BF (2014) Role of silanized halloysite nanotubes on structural, mechanical properties and fracture toughness of thermoset nanocomposites. Mater Des 57:279–288

Balasubramanian K, Burghard M (2006) Biosensors based on carbon nanotubes. Anal Bioanal Chem 385:452–468

Barakat N, Kanjawal M, Chronakis L, Kim H (2013) Influence of temperature on the photodegradation process using Ag-doped TiO_2 nanostructures: negative impact with the nanofibers. J mol Cat A 366:333–340

Bideau B, Bras J, Saini S, Daneault C, Lorangera E (2016) Mechanical and antibacterial properties of a nanocellulose-polypyrrole multilayer composite. Mater Sci Eng C 69:977–984

Cabuk M, Alan Y, Yavuz M, Unal HI (2014) Synthesis, characterization and antimicrobial activity of biodegradable conducting polypyrrole-graft-chitosan copolymer. Appl Surf Sci 318:168–175

Chahal S, Rani N, Kumar A, Kumar P (2019) UV-irradiated photocatalytic performance of yttrium doped ceria for hazardous Rose Bengal dye. Appl Surf Sci 493:87–93

Chahal S, Rani N, Kumar A, Kumar P (2020) Electronic structure and photocatalytic activity of samarium doped cerium oxide nanoparticles for hazardous rose bengal dye degradation. Vacuum 172:109075

Chen X, Zheng Z, Ke X, Jaatinen E, Xi T, Wang D, Guo C, Zhao J, Zhu H (2010) Supported silver nanoparticles as photocatalysts under ultraviolet and visible light irradiation. Green Chem 12:414–419

Chen Z, Shan F, Cao L, Fang G (2012) Synthesis and thermal properties of shape-stabilized lauric acid/activated carbon composites as phase change materials for thermal energy storage. Sol Energ Mat Sol C 102:131–136

Darshna D, Potphode P, Sarada S, Mishra P, Patri M (2015) Polyaniline/partially exfoliated multi-walled carbon nanotubes-based nanocomposites for supercapacitors. Electrochim Acta 155:402–410

Digge M, Moon R, Gattani S (2005) Applications of carbon nanotubes in drug delivery. Int J PharmTech Res 4:839–847

Dizaj SM, Mennati A, Adibkia K (2015) Antimicrobial activity of carbon-based nanoparticles. Adv Pharm Bull 5:19–23

Dolatabadi JE, Yadollah J, Dusan L (2011) Carbon nanotubes as an advanced drug and gene delivery nanosystem. Curr Nanosci 7:297–314

Duan X, Deng J, Wang X, Guo J, Liu P (2016) Preparation of polypyrrole nanocomposites for supercapacitor using spent battery powder as raw materials. Electrochim Acta 210:646–654

Dubal D, Huertas Z, Holze R, Romero P (2016) Growth of polypyrrole nanostructures through reactive templates for energy storage applications. Electrochim Acta 191:346–354

Feng L, Zheng J, Yang H, Guo Y, Lia W, Lia X (2011) Preparation and characterization of polyethylene glycol/active carbon composites as shape-stabilized phase change materials. Sol Energ Mat Sol C 95:644–650

Franci G, Falanga A, Galdiero S, Palomba L, Rai M, Morelli G, Galdiero M (2015) Silver nanoparticles as potential antibacterial agents. Molecules 20:8856–8874

Gong Y, Wang J, Wei Z, Zhang P, Li H, Wang Y (2014) Combination of carbon nitride and carbon nanotubes: synergistic catalysts for energy conversion. Chemsuschem 7:2303–2309

He K, Zeng Z, Chen A, Zeng G, Xiao R, Xu P, Huang Z, Shi J, Hu L, Chen G (2018) Advancement of Ag–graphene based nanocomposites: an overview of synthesis and its applications. Small 14:1–13

Hecel A, Kolkowska P, Krzywoszynska K, Szebesczyk A, Rowinska Z, Magdalena K (2019) Ag+ complexes as potential therapeutic agents in medicine and pharmacy. Curr Med Chem 26:624–647

Huang Y, Tao J, Meng W, Zhua M, Huang Y, Fu Y, Gao Y, Zhia C (2015) Super-high rate stretchable polypyrrole-based supercapacitors with excellent cycling stability. Nano Energy 11:518–525

Ji Z, Shen X, Yang J, Zhu G, Chen K (2014) A novel reduced graphene oxide/Ag/CeO_2 ternary nanocomposite: green synthesis and catalytic properties. Appl Cat B: Env 144:454–461

Kang S, Pinault M, Pfefferle L (2007) Single-walled carbon nanotubes exhibit strong antimicrobial activity. Langmuir 23:8670–8673

Kang YH, Lee UH, Jung IH, Yoon SC, Cho SY (2019) Enhanced thermoelectric performance of conjugated polymer/CNT nanocomposites by modulating the potential barrier difference between conjugated polymer and CNT. Appl Electron Mater 1:1282–1289

Kaushik V, Arya A, Sindhu A, Singh A (2019) Identification, optimization of culture conditions and bioactive potential of Chinese caterpillar mushroom *Ophiocordyceps sinensis* (Ascomycetes)

mycelium isolated from fruiting body. Int J Med Mushrooms 21:931–942
Kumar D, Nain S, Neena PH, Kumar R (2015) CNT reinforced silver nanocomposites: mechanical and electrical studies. Z Naturforsch 70:1–6
Kümmerer K (2009) Antibiotics in the aquatic environment—a review—Part II. Chemosphere 75:435–441
Liang X, Wang P, Li M, Zhang Q, Wang Z, Dai Y, Zhang X, Liu Y, Whangbo MH, Huang B (2018) Adsorption of gaseous ethylene via induced polarization on plasmonic photocatalyst Ag/AgCl/TiO_2 and subsequent photodegradation. Appl Catal B 220:356–361
Magdalane CM, Kaviyarasu K, Vijaya JJ, Siddhardha B, Jeyaraj B (2016) Photocatalytic activity of binary metal oxide nanocomposites of CeO_2/CdO nanospheres: investigation of optical and antimicrobial activity. J photochem Photobio B 163:77–86
Maruthapandi M, Nagvenkar AP, Perelshtein I, Gedanken A (2019) Carbon-dot initiated synthesis of polypyrrole and polypyrrole@CuO micro/nanoparticles with enhanced antibacterial activity. Appl Polym Mater 1:1181–1186
Masumeh S, Seyed G, Shojaosadati A (2016) Evaluation of the antibacterial activity of Ag/Fe_3O_4 nanocomposites synthesized using starch. Carbohydr Polym 144:454–463
Naz S, Mansoor Q, Nisar A, Karim S, Khan M, Ali G, Rahman A, Ahmad M (2019) Silver nanoparticles embedded graphene oxide nanocomposite with enhanced antibacterial and photocatalytic degradation activities. Chemistry select 4:8372–8377
Pant B, Park M, Kim HK, Park SJ (2016) Ag-ZnO photocatalyst anchored on carbon nanofibers: synthesis, characterization, and photocatalytic activities. Synth Met 220:533–537
Rajendran R, Shrestha LK, Minami K, Subramanian M, Jayavel R, Ariga K (2014) Dimensionally integrated nanoarchitectonics for novel composite from 0D, 1D, and 2D nanomaterials: RGO/CNT/CeO_2 ternary nanocomposite with electrochemical performance. J Mater Chem A 2:18480–18487
Salahuddin N, Elbarbary AA, Salem M, Elksass S (2017) Antimicrobial and antitumor activities of 1,2,4-triazoles/polypyrrole chitosan core shell nanoparticles. J Phys Org Chem 30:1–13
Saravanan R, Francisco G, Stephen A (2017) In: Khan MM, et al. (eds) Nanocomposites for visible light-induced photocatalysis. Springer, Berline, pp 19–40
Sasso C, Zeno E, Conil M, Chaussy D, Naceur M, Sandra B, Lingua T, Beneventi D (2010) Highly conducting polypyrrole/cellulose nanocomposite films with enhanced mechanical properties. Macromol Mater Eng 295:934–941
Shaa Y, Mathewa I, Cuia Q, Claya M, Gaoa V, Zhang XJ, Gu Z (2016) Rapid degradation of azo dye methyl orange using hollow cobalt nanoparticles. Chemosphere 144:1530–1535
Sharma G, Kumar A, Naushad V, Kumar A, Al-Muhtaseb H, Dhiman P, Ghfard A, Stadlera FJ, Khand MR (2018) Photoremediation of toxic dye from aqueous environment using monometallic and bimetallic quantum dots-based nanocomposites. J Clean Prod 172:2919–2930
Shi K, Ren M, Zhitomirsky I (2014) Activated carbon-coated carbon nanotubes for energy storage in supercapacitors and capacitive water purification. Sustain Chem Eng 2:1289–1298
Syafiuddin A, Salmiati SMR, Kueh AB, Hadibarata T, Nur H (2017) A review of silver nanoparticles: research trends, global consumption, synthesis, properties, and future challenges. Adv Sci 64:732–756
Tang J, Chen Q, Xu L, Zhang S, Feng L, Cheng L, Xu H, Liu Z (2013) Graphene Oxide−Silver nanocomposite as a highly effective antibacterial agent with species-specific mechanisms. ACS Appl Mater Interf 5:3867–3874
Vajnhandl S, Valh J (2014) The status of water reuse in European textile sector. J Environ Manage 141:29–35
Wan C, Li J (2016) Cellulose aerogels functionalized with polypyrrole and silver nanoparticles: in-situ synthesis, characterization and antibacterial activity. Carbohydr Polym 146:362–367
Wang J, Musameh M (2005) Carbon-nanotubes doped polypyrrole glucose biosensor. Anal Chim Acta 539:209–213
Wang Z, Yin L, Zhang M, Zhou G, Fei H, Shi H, Dai H (2014) Synthesis and characterization of Ag_3PO_4/multiwalled carbon nanotube composite photocatalyst with enhanced photocatalytic activity and stability under visible light. J Mater Sci 49:1585–1593
Wang Y, Lv Z, Liao Q, Shan H, Chen J, Zhou Y, Zhou L, Chen X, Roy V, Wang Z, Xu Z, Zeng Y, Han S (2018a) Synergies of electrochemical metallization and valence change in all inorganic perovskite quantum dots for resistive switching. Adv Mat 30:1–16
Wang Y, Lv Z, Chen J, Wang Z, Zhou Y, Zhou L, Chen X, Han S (2018b) Photonic synapses based on inorganic perovskite quantum dots for neuromorphic computing. Adv. Mat. 30(38):1802883
Wu G, Tan P, Wang D, Li Z, Peng L, Hu Y, Wang C, Zhu W, Chen S, Chen W (2017) High-performance supercapacitors based on electrochemical-induced vertical-aligned carbon nanotubes and polyaniline nanocomposite electrodes. Sci Rep 7:1–8
Xie D, Xia XH, Tang WJ, Zhong Y, Wang YD, Wang DH, Wang XL, Tu JP (2017) Novel carbon channels from loofah sponge for construction of metal sulfide @ carbon composites with robust electrochemical energy storage. J Mater Chem A 5:7578–7585
Yang S, Qua L, Li G, Yang R, Liu C (2010) Gold nanoparticles/ethylenediamine/carbon nanotube modified glassy carbon electrode as the voltammetric sensor for selective determination of rutin in the presence of ascorbic acid. J Electroanal Chem 645:115–122
Yang C, Wei H, Guan L, Guo J, Wang Y, Yan X, Zhang X, Wei S, Guo Z (2015) Polymer nanocomposites for energy storage, energy saving, and anticorrosion. J Mater Chem A 3:14929–14941
Yu L, Zhang Y, Zhang B, Liu J (2015) Enhanced antibacterial activity of silver nanoparticles/halloysite nanotubes/graphene nanocomposites with sandwich-like structure. Sci Rep 4:4551–4556
Yun H, Kim JD, Choi HC, Lee CW (2013) Antibacterial activity of CNT-Ag and GO-Ag nanocomposites against gram-negative and gram-positive bacteria. B Korean Chem Soc 34:3261–3264
Zhang Y, Chen Y, Zhang H, Zhang B, Liu J (2013) Potent antibacterial activity of a novel silver nanoparticle-halloysite nanotube nanocomposite powder. J Inorg Biochem 118:59–64